JACS
JOURNAL OF THE AMERICAN CHEMICAL SOCIETY
Article
pubs.acs.org/JACS

N-Annulated Perylene as An Efficient Electron Donor for Porphyrin-Based Dyes: Enhanced Light-Harvesting Ability and High-Efficiency Co(II/III)-Based Dye-Sensitized Solar Cells

Jie Luo,[†] Mingfei Xu,[‡] Renzhi Li,[‡] Kuo-Wei Huang,[§] Changyun Jiang,[†] Qingbiao Qi,[∥] Wangdong Zeng,[∥] Jie Zhang,[†] Chunyan Chi,[∥] Peng Wang,*[,‡] and Jishan Wu*[,†,∥]

[†]Institute of Materials Research and Engineering, A*STAR, 3 Research Link, Singapore, 117602

[‡]State Key Laboratory of Polymer Physics and Chemistry, Changchun Institute of Applied Chemistry, Chinese Academy of Sciences, Changchun 130022, P.R. China

[§]Division of Physical and Life Sciences and Engineering and KAUST Catalysis Center, King Abdullah University of Science and Technology (KAUST), Thuwal 23955-6900, Saudi Arabia

[∥]Department of Chemistry, National University of Singapore, 3 Science Drive 3, 117543, Singapore

Supporting Information

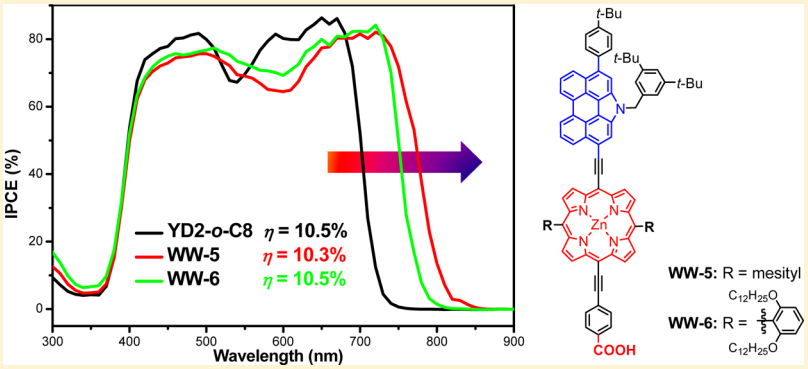

ABSTRACT: Porphyrin-based dyes recently have become good candidates for dye-sensitized solar cells (DSCs). However, the bottleneck is how to further improve their light-harvesting ability. In this work, *N*-annulated perylene (NP) was used to functionalize the Zn-porphyrin, and four "push−pull"-type NP-substituted and fused porphyrin dyes with intense absorption in the visible and even in the near-infrared (NIR) region were synthesized. Co(II/III)-based DSC device characterizations revealed that dyes **WW-5** and **WW-6**, in which an ethynylene spacer is incorporated between the NP and porphyrin core, showed pantochromatic photon-to-current conversion efficiency action spectra in the visible and NIR region, with a further red-shift of about 90 and 60 nm, respectively, compared to the benchmark molecule **YD2-*o*-C8**. As a result, the short-circuit current density was largely increased, and the devices displayed power conversion efficiencies as high as 10.3% and 10.5%, respectively, which is comparable to that of the **YD2-*o*-C8** cell (η = 10.5%) under the same conditions. On the other hand, the dye **WW-3** in which the NP unit is directly attached to the porphyrin core showed a moderate power conversion efficiency (η = 5.6%) due to the inefficient π-conjugation, and the NP-fused dye **WW-4** exhibited even poorer performance due to its low-lying LUMO energy level and nondisjointed HOMO/LUMO profile. Our detailed physical measurements (optical and electrochemical), density functional theory calculations, and photovoltaic characterizations disclosed that the energy level alignment, the molecular orbital profile, and dye aggregation all played very important roles on the interface electron transfer and charge recombination kinetics.

1. INTRODUCTION

Dye-sensitized solar cells (DSCs) have received considerable attention due to their high power-conversion efficiencies, ease of fabrication, and low production costs.[1] Among the various synthetic dyes, porphyrins have been considered to be promising candidates for DSCs because of their superior light-harvesting ability in the visible region and easy chemical tuning of their physical properties.[2] The key to achieving highly efficient DSCs lies in the design and synthesis of stable organic dyes with appropriate push−pull structure. On the basis of this strategy, researchers have focused on the functionalization of the β position[3] or *meso* position[4] of the porphyrin core to generate dyes with appropriate energy levels and strong light-harvesting capabilities in the visible range. Recent development of a zinc porphyrin sensitizer (**YD2-*o*-C8**, Figure 1) co-sensitized with an organic dye (**Y123**) using a cobalt-based electrolyte has attained a power conversion efficiency (η) of

Received: September 8, 2013
Published: December 17, 2013

   dx.doi.org/10.1021/ja409291g | *J. Am. Chem. Soc.* 2014, 136, 265−272

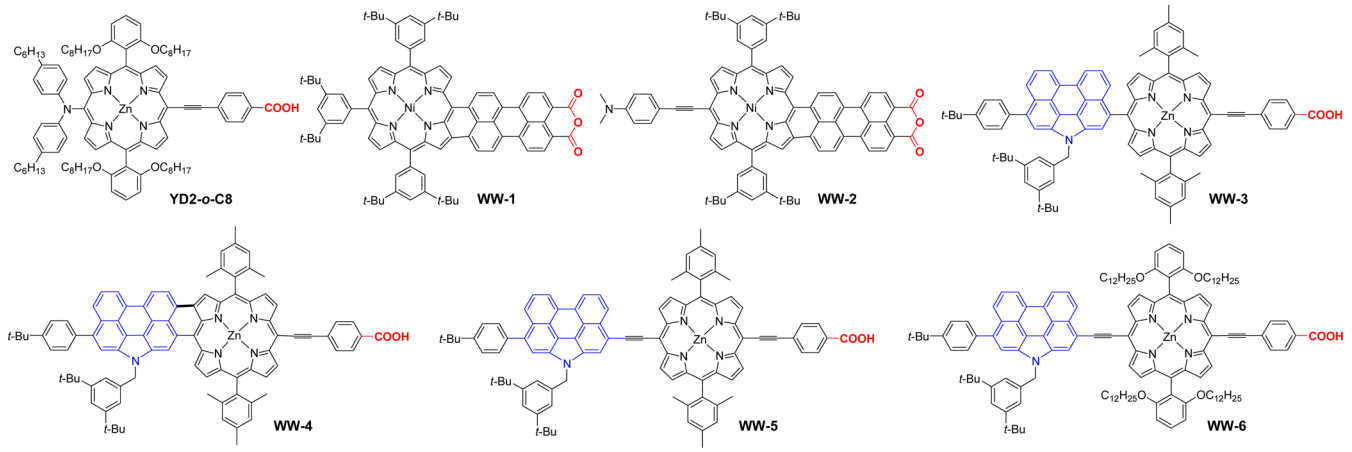

Figure 1. Molecular structures of **YD2-*o*-C8** and a series of perylene-functionalized porphyrin dyes **WW-1**−**WW-6**.

12.3%, which is superior to those based on Ru complexes, setting a new milestone in this area.[5] Further improvement of the device performance will strongly rely on the development of new dyes with even stronger light-harvesting abilities both in the visible (∼400−700) and the near-infrared (NIR) region (∼700−1400 nm). The DSCs based on **YD2-*o*-C8** showed a panchromatic photocurrent response in the whole visible region with the lowest-energy onset at 725 nm,[5] indicating that there is yet plenty of space to further widen the light-harvesting region. One can expect that attachment or fusion of a π-extended chromophore to the porphyrin can further improve its light-harvesting properties. This has been attempted by using cyclic aromatics-substituted porphyrins,[6] porphyrin dimers,[7] and fused porpyrins.[8] Although these dyes showed broad-range light absorption even extended to the NIR region, the device performances are usually not as good as expected, mainly due to dye aggregation and inappropriate energy level alignment. Co-sensitizing has been demonstrated to be an efficient way to improve light-harvesting properties but are usually accompanied by a simultaneous voltage loss.[9] Meanwhile, dye absorption structures play a key role in the device performance and should be considered carefully.[10] Therefore, it is very challenging to design a suitable dye for high-efficiency DSCs. On the one hand, we need organic dyes with strong absorption in the visible and NIR region. On the other hand, the energy level alignment, dye aggregation, surface coverage, charge transfer and recombination kinetics, and excited lifetime of the dyes, etc. all need to be carefully considered.

Among various π-extended polycyclic aromatic hydrocarbons, perylene and its derivatives have been extensively studied due to their excellent photophysical properties (e.g., high extinction coefficient and high fluorescence quantum yield), charge transport properties, as well as outstanding chemical, thermal, and photochemical stability.[11] Furthermore, the availability of their active sites (*peri*- or *bay* positions) leaves room for further chemical modifications. In fact, perylene-based dyes have been successfully used for both organic photovoltaics[12] and DSCs.[13] Therefore, one can expect that functionalization of porphyrin core with a perylene moiety will provide new dyes with largely enhanced light-harvesting ability. Our groups recently reported the synthesis of two perylene anhydride fused porphyrin dyes (**WW-1** and **WW-2**, Figure 1) and their application in DSCs.[14] The devices showed broad incident photon-to-current conversion efficiency (IPCE) action spectra covering the entire visible spectral region and even extending up to 1000 nm. However, only low power conversion efficiencies have been obtained mainly due to their mismatched energy levels, strong dye aggregations and short excited state lifetime. In particular, the low-lying LUMO energy level (−3.92 eV) of both compounds made the electron injection from the photoexcited dyes to the conduction band of the TiO_2 unfavorable. To further modify the structure, we decided to use a new perylene building block, the *N*-annulated perylene (NP), in which the nitrogen atom is annulated at the bay positions.[15] The unique structural character and the electron-rich nature of NP make regioselective functionalization at the *peri*-positions and fusion of this moiety onto other electron-rich units (e.g., NP itself, Zn-porphyrin, BODIPY, etc.) feasible.[16] Moreover, flexible alkyl chains or bulky groups can be readily introduced to the amine site, which can significantly improve its solubility and suppress dye aggregation. In this work, four NP-substituted and fused Zn-porphyrin dyes **WW-3**−**WW-6** (Figure 1) were designed and used in DSCs. The molecular design is based on the following considerations: (1) NP shows strong absorption in visible range (λ_{abs}^{max} = 430 nm) with high fluorescence quantum yield.[17] At the same time, it is a good electron donor, thus a "push−pull" structure is generated in these new dyes; (2) like **YD2-*o*-C8**, the 4-ethynylbenzoic acid was chosen as the acceptor due to its rigid structure and efficient π-conjugation between the donor and acceptor moieties; (3) bulky 3,5-di-*tert*-butylbenzyl, 2,4,6-trimethylphenyl (mesityl) as well as *o*-alkoxy-substituted phenyl groups were chosen to surmount the solubility problem and to reduce dye aggregation.[18] At the same time, they may also retard the interfacial electron back-injection from the conduction band of the nanocrystalline TiO_2 film toward the oxidized redox mediator; (4) for **WW-3** and **WW-4**, the NP unit is directly linked or fused to the Zn-porphyrin core, which allows a good comparison of their physical properties as well as device performance; (5) for **WW-5** and **WW-6**, the introduction of an ethynylene spacer between the NP unit and the porphyrin core leads to an efficient π-conjugation and red-shift of the absorption spectrum compared to **WW-3**, thus improving their light-harvesting properties. The physical properties (optical, electrochemical) of these dyes were investigated by various experimental methods assisted by time-dependent density functional theory (TD DFT) calculations. The DSC devices were fabricated and characterized by using standard liquid cells with Co(II/III) as redox electrolyte. Some of these dyes showed largely enhanced light-harvesting abilities (e.g.,

dx.doi.org/10.1021/ja409291g | *J. Am. Chem. Soc.* 2014, 136, 265−272

WW-5 and WW-6), and as a result, high power conversion efficiencies comparable to that of YD2-*o*-C8 under the same conditions were achieved. Our research also gave a clear structure–property device performance relationship, which is of importance for future design.

2. RESULTS AND DISCUSSION

Synthesis. The synthetic route towards *N*-annulated perylene-substituted and fused porphyrin dyes WW-3–WW-6 is shown in Scheme 1. For WW-3 and WW-4, the synthesis commenced with the preparation of the key precursor **3**, which was synthesized by Suzuki coupling of porphyrin boronic ester **1**[19] and monobrominated *N*-annulated perylene **2**,[16b] followed by bromination with *N*-bromosuccinimide (NBS). Treatment of compound **3** through Sonogashira–Hagihara coupling reaction with 4-ethynylbenzoic acid afforded the NP-substitued Zn-porphyrin WW-3 in 70% yield. $FeBr_3$-promoted intramolecular oxidative cyclodehydrogenation of **3** followed by similar Sonogashira–Hagihara coupling reaction successfully gave the NP-fused Zn-porphyrin WW-4 in 23% yield for two steps. It should be noted that $FeBr_3$ is the key reagent to obtain the fused intermediate **4**. Other synthetic methods such as using $Sc(OTf)_3$/DDQ[16,20] gave complex mixtures, while using $FeCl_3$[21] afforded the cyclized product but with the bromine atom replaced by chlorine, which is unreactive for the subsequent Sonogashira–Hagihara coupling reaction. Synthesis of WW-5 and WW-6 was fulfilled through stepwise Sonogashira–Hagihara coupling reaction of their corresponding dibrominated porphyrin **5a** or **5b** first with ethynyl-substituted *N*-annulated perylene **6** and then with 4-ethynylbenzoic acid. The structures and purity of all the intermediates and the final compounds were identified by NMR and high-resolution mass spectrometry (see Supporting Information [SI]).

Scheme 1. Synthesis of *N*-Annulated Perylene-Substituted and Fused Porphyrin Dyes WW-3–WW-6: (a) $Pd(PPh_3)_4$, Cs_2CO_3; (b) NBS, $CHCl_3$; (c) 4-ethynylbenzoic acid, $Pd(PPh_3)_4$, CuI, TEA; (d) $FeBr_3$, 1,2-dichloroethane; (e) $Pd(PPh_3)_4$, CuI, TEA

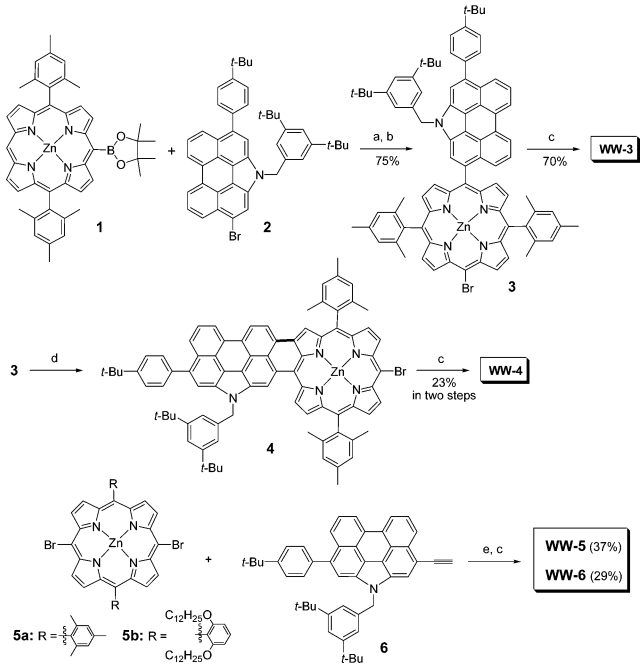

Optical Properties. The absorption spectra of WW-3–WW-6 together with YD2-*o*-C8 in dichloromethane (DCM) are shown in Figure 2, and the data are collected in Table 1.

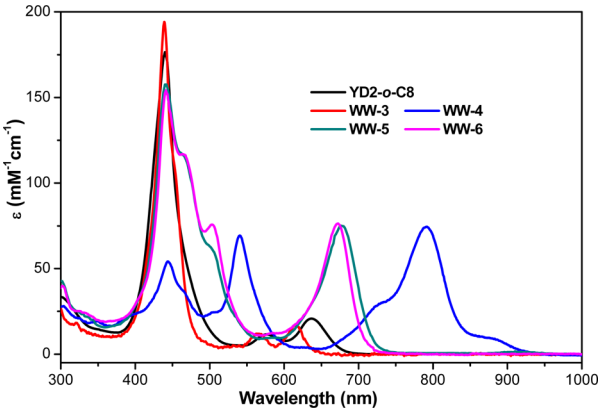

Figure 2. UV–vis–NIR absorption spectra of YD2-*o*-C8 and WW-3–WW-6 in DCM (10^{-5} M).

The absorption spectrum of WW-3 basically is the superimposition of the absorption of the Zn-porphyrin and the NP chromophores, showing an intensive absorption band at 438 nm (ε = 194,700 M^{-1} cm^{-1}) (*p*-band of NP plus the Soret band of porphyrin) and two weak split Q bands at 566 nm (ε = 12,500 M^{-1} cm^{-1}) and 617 nm (ε = 16,700 M^{-1} cm^{-1}), indicating that the NP and the Zn-porphyrin units are weakly coupled. In contrast, the maximum absorption for the NP-fused porphyrin dye WW-4 was much more red-shifted to 792 nm (ε = 75,400 M^{-1} cm^{-1}) due to the efficient π-extension after fusion. Two intense absorption bands at 444 nm (ε = 55,200 M^{-1} cm^{-1}) and 540 nm (ε = 69,900 M^{-1} cm^{-1}) were also observed. The ethynylene-linked dye WW-5 showed a very different absorption spectrum from WW-3. It not only possesses a strong B (or Soret) band with a peak at 441 nm (ε = 158,500 M^{-1} cm^{-1}) and two shoulders at 466 nm (ε = 115,300 M^{-1} cm^{-1}) and 502 nm (ε = 61,500 M^{-1} cm^{-1}), but also an intense and broad Q-band at 679 nm (ε = 75,400 M^{-1} cm^{-1}). The long alkoxy-substituted porphyrin dye WW-6 exhibits a very similar absorption spectrum to that of WW-5, but with a slightly blue-shift of its Q bands (672 nm, ε = 76,900 M^{-1} cm^{-1}). The big difference between WW-5/WW-6 and WW-3 indicated that the incorporation of an ethynylene group between the porphyrin and NP units would help to extend the π-conjugation and decrease the HOMO–LUMO gap, thus giving a longer-wavelength absorption spectrum. Compared to YD2-*o*-C8, both WW-5 and WW-6 gave more intense and red-shifted Q-bands. The optical energy gaps (E_g^{opt}) of WW-3–WW-6 were estimated from the absorption onset as 1.94, 1.33, 1.71, and 1.74 eV, respectively.

Electrochemical Properties. Electrochemical properties of WW-3 to WW-6 were investigated by cyclic voltammetry (CV) and differential pulse voltommetry (DPV) in deoxygenated DCM solution containing 0.1 M tetra-*n*-butylammonium hexafluorophosphate ($TBAPF_6$) as supporting electrolyte (Figure 3 and Figure S1 in SI). The potential was externally calibrated by ferrocenium/ferrocene (Fc^+/Fc) couple and then was calculated versus NHE electrode ($E_{1/2}$ (Fc^+/Fc) = 0.53 V vs Ag/AgCl in our case, and 0.64 V vs NHE). Multiple quasi-

dx.doi.org/10.1021/ja409291g | J. Am. Chem. Soc. 2014, 136, 265–272

Table 1. Summary of Optical and Electrochemical Properties of NP-Functionalized Porphyrin Dyes WW-3–WW-6

dye	λ_{abs} (nm)	ε (M^{-1} cm^{-1})	E_g^{opt} (eV)	$E_{1/2}^{ox}$ (V)	$E_{1/2}^{red}$ (V)	HOMO (eV)	LUMO (eV)	E_g^{EC} (eV)
WW-3	438	194700	1.94	0.85	−1.12	−4.96	−3.09	1.87
	566	12500		1.08	−1.51			
	617	16700		1.49				
WW-4	444	55200	1.33	0.83	−0.54	−4.76	−3.60	1.16
	540	69900		1.11	−1.03			
	792	75400						
WW-5	441	158500	1.71	0.74	−0.96	−4.86	−3.27	1.59
	466	115300		0.97	−1.31			
	502	61500		1.58				
	679	75400		1.78				
WW-6	441	153800	1.74	0.84	−1.22	−4.90	−3.15	1.75
	467	116900		1.06	−1.59			
	503	75800		1.56				
	672	76900		1.82				

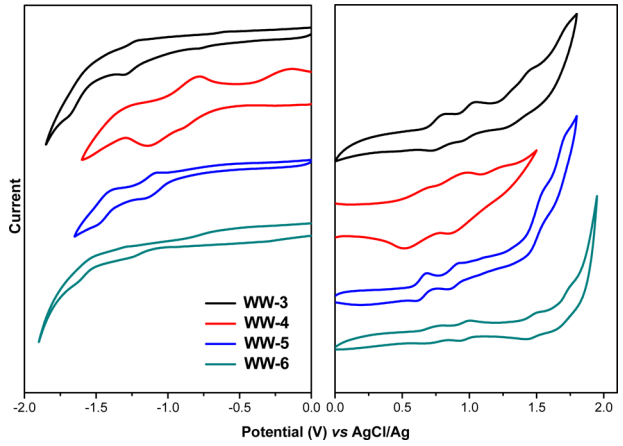

Figure 3. Cyclic voltammograms of **WW-3–WW-6** in dry DCM with $TBAPF_6$ as supporting electrolyte, AgCl/Ag as reference electrode, Au disk as working electrode, Pt wire as counter electrode, and scan rate at 50 mV/s.

reversible or irreversible redox waves were observed for all four compounds (see the list of half wave potentials $E_{1/2}^{ox}$ (anodic scan) and $E_{1/2}^{red}$ (cathodic scan) in Table 1, vs NHE). The HOMO and LUMO energy levels were estimated from the onset of the first oxidation and reduction wave respectively.[22] The measured HOMO energy level of the Co(II)-bpy cation is −4.63 eV and the theoretical LUMO energy level of the isolated TiO_2 nanoparticle is −3.44 eV.[23] The low-lying LUMO energy level of **WW-4** indicates that its driving force for electron injection may not be sufficient. The electrochemical energy gaps (E_g^{EC}) were calculated accordingly to be 1.87, 1.16, 1.59, and 1.75 eV, which are in agreement with the optical energy gap values.

Thus, fusion of a NP unit to the porphyrin core (in **WW-4**) significantly lowers the LUMO and lifts up the HOMO compared to the NP-substituted porphyrin **WW-3**, leading to a narrowed energy gap. Putting additional ethynylene linker between the NP and porphyrin units (in **WW-5** and **WW-6**) also results in a decrease of LUMO and slight up-lift of HOMO, accompanied with a diminished energy gap. Replacement of the mesityl groups in **WW-5** by 2,6-didodecoxyphenyl units in **WW-6** leads to a slight up-lift of the LUMO and an slight increase of the energy gap (by 0.13 eV), which is in consistence with the observed slight blue-shift in the absorption spectrum. For comparison, dye **YD2-*o*-C8** measured under similar conditions has a HOMO of −4.92 eV and LUMO of −3.00 eV, with an E_g^{EC} of 1.92 eV.[5]

TD DFT Calculations. In order to gain better understanding of the molecular geometries, molecular orbitals, optical properties, and electronic properties of the porphyrin dyes **WW-3–WW-6**, TD DFT calculations at the B3LYP/6-31G** level of theory were performed. Figure 4 shows their optimized molecular structures and frontier molecular orbital profiles together with the calculated energy levels of HOMOs and LUMOs. The HOMO of **WW-3** is mainly localized on the NP moiety, while its LUMO is homogeneously distributed through the porphyrin core and the acid binding group. Such an orbital partition feature is due to the nearly orthogonal arrangement of

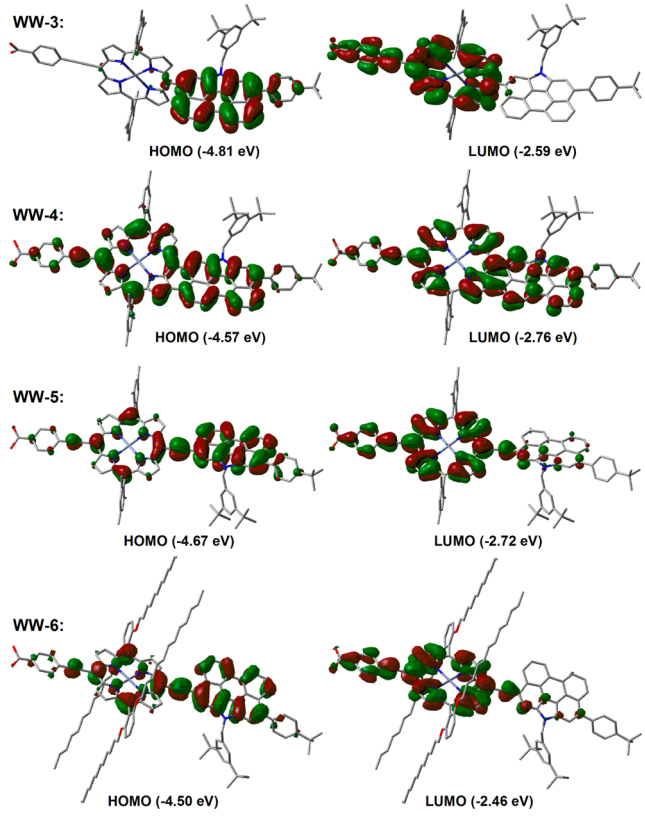

Figure 4. Calculated HOMO and LUMO profiles and energy levels of **WW-3–WW-6** (B3LYP/6-31G**).

dx.doi.org/10.1021/ja409291g | J. Am. Chem. Soc. 2014, 136, 265–272

the NP and porphyin unit which does not allow sufficient π-orbital overlap for extended π-conjugation, in agreement with the superimposition character of the absorption spectrum. For the fused dye **WW-4**, both the HOMO and LUMO are delocalized throughout the highly conjugated backbone. The HOMO and LUMO are not well segregated, and the electrons are less distributed on the acid binding moiety in LUMO, implying that it may be difficult for the photoexcited electrons to inject into the conduction band of TiO_2 via the carboxylic group adsorbed on the TiO_2 surface. For both **WW-5** and **WW-6**, HOMO and LUMO showed a disjointed character, with the HOMO delocalized along both the perylene moiety and porphyrin core, and the LUMO delocalized through the porphyrin core and the acid binding group. Hence, the introduction of ethynylene group between the porphyrin core and NP unit in **WW-5** and **WW-6** is believed to give a better overlap between donor and acceptor moieties, thus providing a fast charge transfer transition. At the same time, the LUMO electron distributions of **WW-5** and **WW-6** share a pattern similar to that of**WW-3**; therefore, electron injection from the carboxylic group into the conduction band of TiO_2 will not be affected significantly. The didodecoxyphenyl groups in **WW-6** are nearly perpendicular to the porphyin plane and envelop the porphyrin core, which may help to suppress the dye aggregation and also slightly lift up the HOMO and LUMO as demonstrated by Lin and Yeh et al.[5,18d] The calculations also predict that **WW-3**−**WW-6** show the longest-wavelength absorption maximum at 569.9, 739.6, 715.8, and 684.1 nm, respectively, (Figures S2−S5 in SI), which follow the same trend with the experimental observations.

Photovoltaic Properties. The newly synthesized dyes were adsorbed onto a bilayer (4.2 + 5.0 μm) titania film[24] by using an optimized binary solvent system of THF and ethanol (volume ratio 1:4) to serve as a working electrode for photovoltaic characterizations. Our cobalt electrolyte is composed of 0.25 M tris(2,2′-bipyridine) cobalt(II) di[bis-(trifluoromethanesulfonyl)imide], 0.05 M tris(2,2′-bipyridine)-cobalt(III) tris[bis(trifluoromethanesulfonyl)imide], 0.5 M 4-*tert*-butylpyridine (TBP), and 0.1 M lithium bis-(trifluoromethanesulfonyl)imide (LiTFSI) in acetonitrile. Figure 5 shows the photocurrent density−voltage (J−V) characteristics and the corresponding IPCE action spectra for **WW-3**−**WW-6** cells measured under standard photovoltaic reporting conditions (global AM1.5 sunlight with irradiance of 100 mW cm^{-2} at 298 K), with **YD2-*o*-C8** as the reference cell. The photovoltaic parameters under various irradiances (G) are listed in Table 2. The J_{sc}^{cal} values calculated from IPCE are also shown for comparison with the measured J_{SC} to confirm the accuracy of the energy conversion efficiency.

When **WW-3** was tested for the photovoltaic performance, it only showed a moderate power conversion efficiency of 5.6%, which can be mainly attributed to the low short-circuit current (J_{sc}) value (9.81 mA cm^{-1}). Dye **WW-3** showed IPCE values exceeding 35% from 390 nm up to 666 nm, with a big gap at the middle, which is consistent with its absorption spectrum. The highest IPCE value can reach 73% at 458 nm, indicating an efficient electron injection from the photoexcited dyes to the conduction band of the TiO_2. However, the moderate light-harvesting ability limits the J_{sc} value and eventually the efficiency. Dye **WW-4** showed even worse device performance under the same condition. A very weak photocurrent response was observed, although its absorption spectrum is extended to the NIR region up to 920 nm. Both the J_{sc} and open-circuit

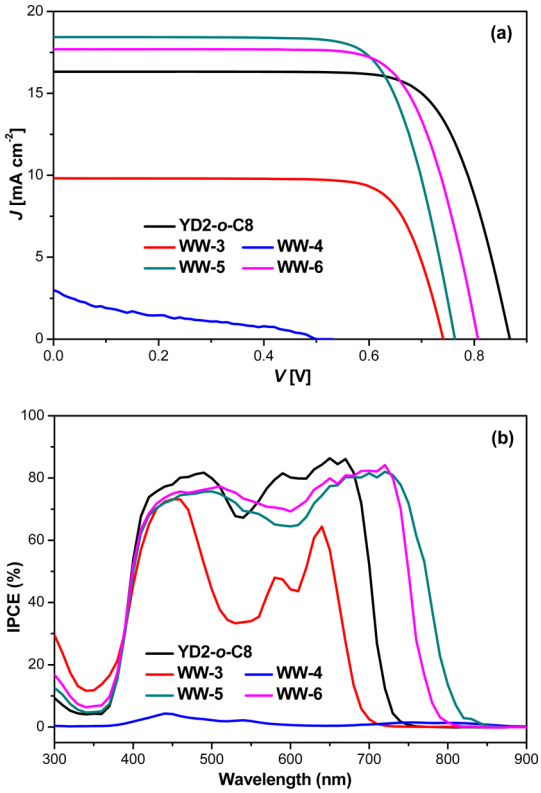

Figure 5. (a) Current−voltage characteristics of the **WW-3**−**WW-6**-sensitzed solar cells and the **YD2-*o*-C8** cell and (b) the corresponding IPCE action spectra.

voltage (V_{oc}) gave very disappointing results (3.00 mA cm^{-1} and 0.500 V, respectively). The relatively low efficiency presumably ascribed to its low-lying LUMO energy level (−3.60 eV) and the nondisjointed character of its HOMO/LUMO profiles, which make the electron injection from the excited dyes to the conduction edge TiO_2 much less efficient. Fortunately, dyes **WW-5** and **WW-6**, possessing an ethynylene bridge between the porphyrin core and the perylene moiety, exhibited much better performances which are comparable to that of the benchmark molecule **YD2-*o*-C8**. Indeed, when **WW-5** was employed, an impressive broad IPCE action spectrum covering the pantochromatic visible region and part of the NIR region was achieved. The IPCE values are high (>65% from 410 to 760 nm) and comparable to that of **YD2-*o*-C8**. The most distinct character is that the onset of IPCE action spectrum was further red-shifted from 725 nm for **YD2-*o*-C8** cell to 815 nm for **WW-5** cell; as a result, a high J_{sc} of 18.4 mA cm^{-2} was achieved for **WW-5**-sensitized solar cells, in comparison to a J_{sc} of 16.33 mA cm^{-2} for the **YD2-*o*-C8** cell. The V_{oc} value of **WW-5** cell (0.766 V), however, is lower than that of the latter (0.868 V), and its fill factor (FF) is also slightly lower; as a result, the overall power conversion efficiency of the **WW-5** cell reached 10.3%, which is very close to that of **YD2-*o*-C8** cell (η = 10.5%) at the same testing condition. The **WW-6**-based cell showed a similar pantochromatic IPCE action spectrum with the onset (785 nm) blue-shifted compared to that of **WW-5** cell, which is consisent with their absorption spectra. Accordingly, the J_{sc} value decreased to 17.69 mA cm^{-2}. The V_{oc} (0.809 V), however, was significantly improved, and the power conversion efficiency was as high as 10.5%, which is the same for the **YD2-*o*-C8** cell. Under a lower irradiation

dx.doi.org/10.1021/ja409291g | J. Am. Chem. Soc. 2014, 136, 265−272

Table 2. Photovoltaic Parameters of Cells Measured at Various Irradiances (G) of Simulated AM1.5 Sunlight

dye	G [mW cm^{-2}]	J_{sc}^{cal} [mA cm^{-2}]	J_{sc} [mA cm^{-2}]	V_{oc} [V]	FF	η [%]
YD2-*o*-C8	12.58	2.03	2.03	0.781	0.791	10.0
	23	3.72	3.79	0.810	0.786	10.5
	50	8.09	8.31	0.842	0.773	10.8
	100	16.17	16.33	0.868	0.743	10.5
WW-3	100	9.40	9.81	0.744	0.767	5.6
WW-4	100	4.52	3.00	0.500	0.299	0.3
WW-5	12.58	2.37	2.39	0.698	0.779	10.3
	23	4.34	4.44	0.719	0.780	10.8
	50	9.44	9.71	0.746	0.766	11.1
	100	18.87	18.43	0.766	0.733	10.3
WW-6	12.58	2.31	2.32	0.730	0.777	10.5
	23	4.22	4.31	0.755	0.776	11.0
	50	9.17	9.42	0.786	0.762	11.3
	100	18.34	17.69	0.809	0.735	10.5

condition at G = 50 mW cm^{-2}, the η values of the **WW-5** (η = 11.1%) and **WW-6** cells (η = 11.3) were even higher than that of **YD2-*o*-C8** cell (η = 10.8%) (Table 2).

In order to understand the performance differences from a chemistry perspective, a dye-loading density study of porphyrin dyes on TiO_2 film was conducted. **WW-3**–**WW-6** gave dye-loading densities of 1.69×10^{-8}, 1.84×10^{-8}, 1.81×10^{-8}, and 1.62×10^{-8} cm^{-2} μm^{-1}, respectively. In comparison, **YD2-*o*-C8** gave a relative lower density of 1.38×10^{-8} cm^{-2} μm^{-1}, indicating a higher power conversion ability of this dye. We also conducted electronic absorption spectra of 4-μm-thick, transparent dye-grafted titania films immersed in the Co-bpy electrolyte (Figure S6 in SI). The results indicate that the IPCE difference is not induced by the light absorption abilities.

To further understand the dye structure–device performance relationship, we conducted further physical measurements on the **WW-5** and the **WW-6** cells with the **YD2-*o*-C8** cell as a reference. For a short-circuit DSC device, it is known that the J_{sc} is measured at the condition of a considerable low electron density in the nanocrystalline titania film, and the charge recombination flux is significantly reduced. Thereby, the measured J_{sc} is roughly proportional to the photocarrier generation flux. The validity of this analysis motivated us to compare the dye structure-correlated V_{oc} variation at a given J_{sc} by measuring J–V curves under various light intensities and plotting V_{oc} as a function of J_{sc} (Figure 6). It is noted that at a given J_{sc}, the **YD2-*o*-C8** cell exhibits a higher V_{oc} than **WW-6**, while **WW-5** gives the lowest V_{oc} value.

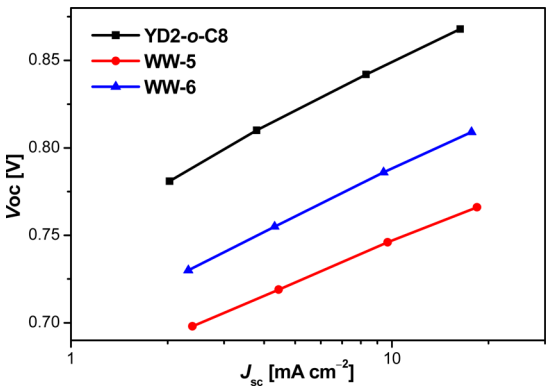

Figure 6. Open-circuit photovoltage plotted as a function of short-circuit photocurrent density.

It is widely recognized that for a fixed redox electrolyte in DSCs, the rise or fall of V_{oc} is determined by the titania electron quasi-Fermi-level ($E_{F,n}$), which intrinsically stems from a change of titania conduction band edge (E_c) and/or a variation of titania electron density.[25] At a given flux of photocarrier generation, the titania electron density is determined by the interfacial recombination rate of titania electrons with electron-accepting species in electrolytes and/or dye cations. Thereby charge extraction and transient photovoltage decay measurements were further carried out to understand the electronic origins of the aforesaid V_{oc} fluctuation. As shown in Figure 7a, the cells made with **YD2-*o*-C8**, **WW-5**, and **WW-6** feature a similar extracted charge (Q) at the same potential bias V_{oc},

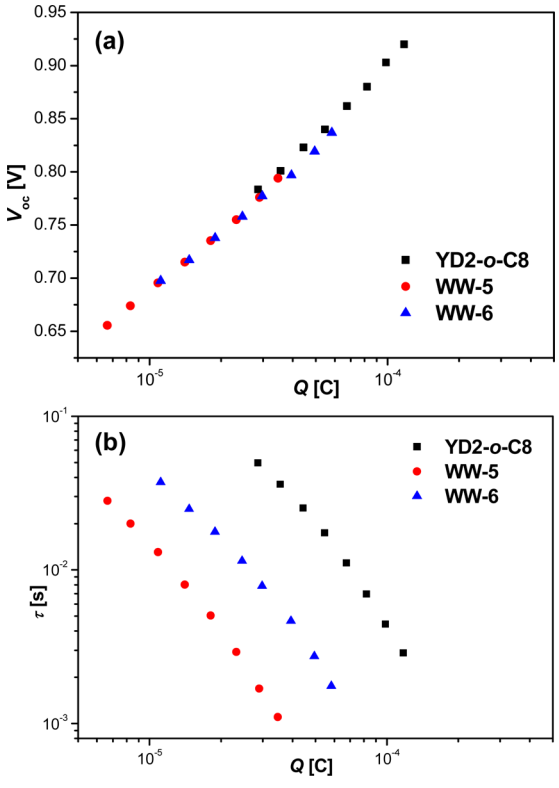

Figure 7. (a) Comparison of the charges extracted from the dye-grafted titania films at a certain open-circuit photovoltage. (b) Comparisons of electron lifetime at a given open-circuit photovoltage.

dx.doi.org/10.1021/ja409291g | J. Am. Chem. Soc. 2014, 136, 265–272

suggesting a fixed conduction-band edge of titania with respect to the electrolyte Fermi-level. As Figure 7b presents, the **YD2-*o*-C8** cell displays longer charge recombination lifetime (τ_n) than **WW-6** and **WW-5** cells at a given charge Q, accounting for the aforementioned more superior photovoltage at a given J_{sc} for **YD2-*o*-C8** than for **WW-6**, followed by that for **WW-5**. The observed higher V_{oc} for **WW-6** cell as compared to **WW-5** cell could be ascribed to the efficient suppression of dye aggregation as well as the retardance of charge recombination between the TiO_2 film and the Co(II/III) redox electrolyte. In addition, the slight rise of the HOMO of **WW-5** in comparison to that of **WW-6** may be another reason, which could diminish the dye regeneration. Compared to **YD2-*o*-C8**, **WW-6** has a very similar HOMO energy level but with a lower-lying LUMO, which could make the electron injection to the TiO_2 film at a slower rate.

The short-circuit currents of the **YD2-*o*-C8**, **WW-5** and **WW-6** cell increase linearly with light intensity up to about 1 sun, and this is illustrated in Figure 8. This linearity shows that the photocurrent is not limited by diffusion of the cobalt electrolyte within the nanocrystalline film.

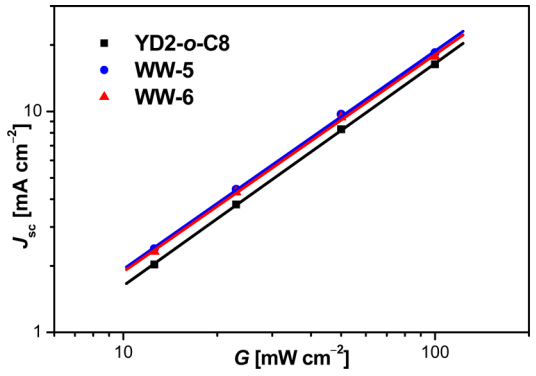

Figure 8. Plots of short-circuit photocurrent density versus incident light intensity. The experimental data are fitted to a power function $J_{sc} \propto G^{\alpha}$, affording the α values of 1.0060 for **YD2-*o*-C8**, 0.9875 for **WW-5** and 0.9825 for **WW-6**.

3. CONCLUSION

In summary, we have designed and synthesized a series of "push−pull" type *N*-annulated perylene-functionalized porphyrin dyes **WW-3**−**WW-6** which displayed intense absorption in the visible and even in the NIR spectral range. Although the fully fused dye **WW-4** showed the best light-harvesting ability, DSC devices based on this dye revealed poor performances due to its low-lying LUMO energy level and nondisjointed HOMO/LUMO profiles, which leads to insufficient driving force for electron injection. Compared with the NP directly substituted dye **WW-3**, the ethynylene bridged NP and porphyrin dyads **WW-5** and **WW-6** exhibited improved π-conjugation and red-shifted absorption spectra. As a result, the DSCs based on these two dyes showed pantochromatic IPCE action spectra with the onset red-shifted about 90 and 60 nm, respectively, compared to the **YD2-*o*-C8** cell. Consequently, the short circuit current J_{sc} values have been significantly improved. The power conversion efficiencies of the cells based on these two new dyes reached as high as 10.5% under simulated AM 1.5 global sunlight, which is comparable to the **YD2-*o*-C8** cell (η = 10.5%) under similar conditions. The device parameters of dyes can be correlated to their light-harvesting abilities, molecular orbital profiles, energy level alignment, and dye aggregation, all of which are important factors we must carefully consider. Further work to improve device performance by using new dyes with even better light-harvesting abilities and optimized energy levels is underway in our laboratories.

■ ASSOCIATED CONTENT

Supporting Information

Synthetic procedures and characterization data of all new compounds. Details for all physical characterizations and theoretical calculations. Photovoltaic test procedure and mechanism studies. This material is available free of charge via the Internet at http://pubs.acs.org.

■ AUTHOR INFORMATION

Corresponding Authors

chmwuj@nus.edu.sg or wuj@imre.a-star.edu.sg
peng.wang@ciac.jl.cn

Notes

The authors declare no competing financial interest.

■ ACKNOWLEDGMENTS

J.W. acknowledges financial support from the IMRE Core Funding (IMRE/13-1C0205) and MOE Tier 2 grant (MOE2011-T2-2-130). P.W. thanks the National 973 Program (No. 2011CBA00702) and the National Science Foundation of China (No. 51203150). K.-W.H. acknowledges financial support from KAUST.

■ REFERENCES

(1) (a) Oregan, B.; Grätzel, M. *Nature* **1991**, *353*, 737. (b) Imahori, H.; Umeyama, T.; Ito, S. *Acc. Chem. Res.* **2009**, *42*, 1809. (c) Hagfeldt, A.; Boschloo, G.; Sun, L.; Kloo, L.; Pettersson, H. *Chem. Rev.* **2010**, *110*, 6595. (d) Hardin, B. E.; Snaith, H. J.; McGehee, M. D. *Nature Photon.* **2012**, *6*, 162. (e) Zhang, S.; Yang, X.; Numata, Y.; Han, L. *Energy Environ. Sci.* **2013**, *6*, 1443.

(2) (a) Walter, M. G.; Rudine, A. B.; Wamser, C. C. *J. Porphyrins Phthalocyanines* **2010**, *14*, 760. (b) Li, L.-L.; Diau, E. W.-G. *Chem. Soc. Rev.* **2013**, *42*, 291.

(3) (a) Kay, A.; Grätzel, M. *J. Phys. Chem.* **1993**, *97*, 6272. (b) Nazeeruddin, M. K.; Humphry-Baker, R.; Officer, D. L.; Campbell, W. M.; Burrell, A. K.; Grätzel, M. *Langmuir* **2004**, *20*, 6514. (c) Wang, Q.; Carnpbell, W. M.; Bonfantani, E. E.; Jolley, K. W.; Officer, D. L.; Walsh, P. J.; Gordon, K.; Humphry-Baker, R.; Nazeeruddin, M. K.; Grätzel, M. *J. Phys. Chem. B* **2005**, *109*, 15397. (d) Campbell, W. M.; Jolley, K. W.; Wagner, P.; Wagner, K.; Walsh, P. J.; Gordon, K. C.; Schmidt-Mende, L.; Nazeeruddin, M. K.; Wang, Q.; Grätzel, M.; Officer, D. L. *J. Phys. Chem. C* **2007**, *111*, 11760. (e) Park, J. K.; Lee, H. R.; Chen, J. P.; Shinokubo, H.; Osuka, A.; Kim, D. *J. Phys. Chem. C* **2008**, *112*, 16691. (f) Ishida, M.; Park, S. W.; Hwang, D.; Koo, Y. B.; Sessler, J. L.; Kim, D. Y.; Kim, D. *J. Phys. Chem. C* **2011**, *115*, 19343.

(4) (a) Lin, V.; DiMagno, S.; Therien, M. *Science* **1994**, *264*, 1105. (b) Cherian, S.; Wamser, C. C. *J. Phys. Chem. B* **2000**, *104*, 3624. (c) Screen, T. E. O.; Lawton, K. B.; Wilson, G. S.; Dolney, N.; Ispasoiu, R.; Goodson, T., III.; Martin, S. J.; Bradley, D. D. C.; Anderson, H. L. *J. Mater. Chem.* **2001**, *11*, 312. (d) Rochford, J.; Chu, D.; Hagfeldt, A.; Galoppini, E. *J. Am. Chem. Soc.* **2007**, *129*, 4655. (e) Stromberg, J. R.; Marton, A.; Kee, H. L.; Kirmaier, C.; Diers, J. R.; Muthiah, C.; Taniguchi, M.; Lindsey, J. S.; Bocian, D. F.; Meyer, G. J.; Holten, D. *J. Phys. Chem. C* **2007**, *111*, 15464. (f) Eu, S.; Hayashi, S.; Umeyama, T.; Oguro, A.; Kawasaki, M.; Kadota, N.; Matano, Y.; Imahori, H. *J. Phys. Chem. C* **2007**, *111*, 3528. (g) Lu, H. P.; Tsai, C. Y.; Yen, W. N.; Hsieh, C. P.; Lee, C. W.; Yeh, C. Y.; Diau, E. W. G. *J. Phys. Chem. C* **2009**, *113*, 20990. (h) Hsieh, C.-P.; Lu, H.-P.; Chiu, C.-

L.; Lee, C.-W.; Chuang, S.-H.; Mai, C.-L.; Yen, W.-N.; Hsu, S.-J.; Diau, E. W.-G.; Yeh, C.-Y. *J. Mater. Chem.* **2010**, *20*, 1127.
(5) Yella, A.; Lee, H. W.; Tsao, H. N.; Yi, C.; Chandiran, A. K.; Nazeeruddin, M. K.; Diau, E. W.-G.; Yeh, C. Y.; Zakeeruddin, S. M.; Grätzel, M. *Science* **2011**, *334*, 629.
(6) (a) Lu, H. P.; Mai, C. L.; Tsia, C. Y.; Hsu, S. J.; Hsieh, C. P.; Chiu, C. L.; Yeh, C. Y.; Diau, E. W.-G. *Phys. Chem. Chem. Phys.* **2009**, *11*, 10270. (b) Lin, C.-Y.; Wang, Y.-C.; Hsu, S.-J.; Lo, C.-F.; Diau, E. W.-G. *J. Phys. Chem. C* **2010**, *114*, 687. (c) Wang, C.-L.; Chang, Y.-C.; Lan, C.-M.; Lo, C.-F.; Diau, E. W.-G.; Lin, C.-Y. *Energy Environ. Sci.* **2011**, *4*, 1788. (d) Wu, C. H.; Pan, T. Y.; Hong, S. H.; Wang, C. L.; Kuo, H. H.; Chu, Y. Y.; Diau, E. W.-G.; Lin, C. Y. *Chem. Commun.* **2012**, *48*, 4329.
(7) (a) Mozer, A. J.; Griffith, M. J.; Tsekouras, G.; Wagner, P.; Wallace, G. G.; Mori, S.; Sunahara, K.; Miyashita, M.; Earles, J. C.; Gordon, K. C.; Du, L. C.; Katoh, R.; Furube, A.; Officer, D. L. *J. Am. Chem. Soc.* **2009**, *131*, 15621. (b) Park, J. K.; Chen, J. P.; Lee, H. R.; Park, S. W.; Shinokubo, H.; Osuka, A.; Kim, D. *J. Phys. Chem. C* **2009**, *113*, 21956. (c) Mai, C. L.; Huang, W. K.; Lu, H. P.; Lee, C. W.; Chiu, C. L.; Liang, Y. R.; Diau, E. W.-G.; Yeh, C. Y. *Chem. Commun.* **2010**, *46*, 809. (d) Liu, Y.; Lin, H.; Dy, J. T.; Tamaki, K.; Nakazaki, J.; Nakayama, D.; Uchida, S.; Kubo, T.; Segawa, H. *Chem. Commun.* **2011**, *47*, 4010.
(8) (a) Tanaka, M.; Hayashi, S.; Eu, S.; Umeyama, T.; Matano, Y.; Imahori, H. *Chem. Commun.* **2007**, *43*, 2069. (b) Hayashi, S.; Tanaka, M.; Hayashi, H.; Eu, S.; Umeyama, T.; Matano, Y.; Araki, Y.; Imahori, H. *J. Phys. Chem. C* **2008**, *112*, 15576. (c) Hayashi, S.; Matsubara, Y.; Eu, S.; Hayashi, H.; Umeyama, T.; Matano, Y.; Imahori, H. *Chem. Lett.* **2008**, *37*, 846. (d) Eu, S.; Hayashi, S.; Umeyama, T.; Matano, Y.; Araki, Y.; Imahori, H. *J. Phys. Chem. C* **2008**, *112*, 4396.
(9) Shrestha, M.; Si, L. P.; Chang, C. W.; He, H. S.; Sykes, A.; Lin, C. Y.; Diau, E. W.-G. *J. Phys. Chem. C* **2012**, *116*, 10451.
(10) (a) Imahori, H.; Kang, S.; Hayashi, H.; Haruta, M.; Kurata, H.; Isoda, S.; Canton, S. E.; Infahsaeng, Y.; Kathiravan, A.; Pascher, T.; Chábera, P.; Yartsev, A. P.; Sundström, V. *J. Phys. Chem. A* **2011**, *115*, 3679. (b) Ye, S.; Kathiravan, A.; Hayashi, H.; Tong, Y.; Infahsaeng, Y.; Chabera, P.; Pascher, T.; Yartsev, A. P.; Isoda, S.; Imahori, H.; Sundström, V. *J. Phys. Chem. C* **2013**, *117*, 6066.
(11) (a) Tang, C. W. *Appl. Phys. Lett.* **1986**, *48*, 183. (b) Schmidt-Mende, L.; Fechtenköter, A.; Müllen, K.; Moons, E.; Friend, R. H.; MacKenzie, J. D. *Science* **2001**, *293*, 1119. (c) Zhan, X.; Tan, Z.; Domercq, B.; An, Z.; Zhang, X.; Barlow, S.; Li, Y.; Zhu, D.; Kippelen, B.; Marder, S. R. *J. Am. Chem. Soc.* **2007**, *129*, 7246.
(12) (a) Cremer, J.; Mena-Osteritz, E. M.; Pschierer, N. G.; Müllen, K.; Bauerle, P. *Org. Biomol. Chem.* **2005**, *3*, 985. (b) Cremer, J.; Bauerle, P. *Eur. J. Org. Chem.* **2005**, 3715. (c) Cremer, J.; Bauerle, P. *J. Mater. Chem.* **2006**, *16*, 874. (d) Zhan, X. W.; Tan, Z. A.; Domercq, B.; An, Z. S.; Zhang, X.; Barlow, S.; Li, Y. F.; Zhu, D. B.; Kippelen, B.; Marder, S. R. *J. Am. Chem. Soc.* **2007**, *129*, 7246. (e) Tan, Z. A.; Zhou, E. J.; Zhan, X. W.; Wang, X.; Li, Y. F.; Barlow, S.; Marder, S. R. *Appl. Phys. Lett.* **2008**, *93*, 073309. (f) Zhan, X. W.; Tan, Z. A.; Zhou, E. J.; Li, Y. F.; Misra, R.; Grant, A.; Domercq, B.; Zhang, X. H.; An, Z. S.; Zhang, X.; Barlow, S.; Kippelen, B.; Marder, S. R. *J. Mater. Chem.* **2009**, *19*, 5794. (g) Mikroyannidis, J. A.; Stylianakis, M. M.; Suresh, P.; Sharma, G. D. *Sol. Energy Mater. Sol. Cells* **2009**, *93*, 1792. (h) Sharma, G. D.; Balraju, P.; Mikroyannidis, J. A.; Stylianakis, M. M. *Sol. Energy Mater. Sol. Cells* **2009**, *93*, 2025. (i) Sharma, G. D.; Suresh, P.; Mikroyannidis, J. A.; Stylianakis, M. M. *J. Mater. Chem.* **2010**, *20*, 561.
(13) (a) Ferrere, S.; Zaban, A.; Gregg, B. A. *J. Phys. Chem. B* **1997**, *101*, 4490. (b) Ferrere, S.; Gregg, B. A. *New J. Chem.* **2002**, *26*, 1155. (c) Edvinsson, T.; Li, C.; Pschirer, N.; Schoneboom, J.; Eickemeyer, F.; Sens, R.; Boschloo, G.; Herrmann, A.; Müllen, K.; Hagfeldt, A. *J. Phys. Chem. C* **2007**, *111*, 15137. (d) Shibano, Y.; Umeyama, T.; Matano, Y.; Imahori, H. *Org. Lett.* **2007**, *9*, 1971. (e) Edvinsson, T.; Li, C.; Pschirer, N.; Schöneboom, J.; Eickemeyer, F.; Sens, R.; Boschloo, G.; Herrmann, A.; Müllen, K.; Hagfeldt, A. *J. Phys. Chem. C* **2007**, *111*, 15137. (f) Fortage, J.; Séverac, M.; Houarner-Rassin, C.; Pellegrin, Y.; Blart, E.; Odobel, F. *J. Photochem. Photobiol. A* **2008**, *197*, 156. (g) Li, C.; Yum, J.-H.; Moon, S.-J.; Herrmann, A.; Eickemeyer, F.; Pschirer, N. G.; Erk, P.; Schöneboom, J.; Müllen, K.; Grätzel, M.; Nazeeruddin, M. K. *ChemSusChem* **2008**, *1*, 615. (h) Jin, Y. H.; Hua, J. L.; Wu, W. J.; Ma, X. M.; Meng, F. S. *Synth. Met.* **2008**, *158*, 64. (i) Planells, M.; Cespedes-Guirao, F. J.; Goncalves, L.; Sastre-Santos, A.; Fernandez-Lazaro, F.; Palomares, E. *J. Mater. Chem.* **2009**, *19*, 5818. (j) Li, C.; Liu, Z. H.; Schoneboom, J.; Eickemeyer, F.; Pschirer, N. G.; Erk, P.; Herrmann, A.; Müllen, K. *J. Mater. Chem.* **2009**, *19*, 5405. (k) Imahori, H.; Mathew, S. *J. Mater. Chem.* **2011**, *21*, 7166.
(14) Jiao, C.; Zu, N.; Huang, K.-W.; Wang, P.; Wu, J. *Org. Lett.* **2011**, *13*, 3652.
(15) (a) Looker, J. J. *J. Org. Chem.* **1972**, *37*, 3379. (b) Jiang, W.; Qian, H.; Li, Y.; Wang, Z. *J. Org. Chem.* **2008**, *73*, 7369.
(16) (a) Li, Y.; Wang, Z. *Org. Lett.* **2009**, *11*, 1385. (b) Jiao, C.; Huang, K.-W.; Luo, J.; Zhang, K.; Chi, C.; Wu, J. *Org. Lett.* **2009**, *11*, 4508. (c) Li, Y.; Gao, J.; Motta, S. D.; Negri, F.; Wang, Z. *J. Am. Chem. Soc.* **2010**, *132*, 4208. (d) Jiao, C.; Huang, K.-W.; Guan, Z.; Xu, Q.-H.; Wu, J. *Org. Lett.* **2010**, *12*, 4046. (e) Jiao, C.; Huang, K.-W.; Wu, J. *Org. Lett.* **2011**, *13*, 632. (f) Zeng, Z.; Ishida, M.; Zafra, J. L.; Zhu, X.; Sung, Y. M.; Bao, N.; Webster, R. D.; Lee, B. S.; Li, R.-W.; Zeng, W.; Li, Y.; Chi, C.; Navarrete, J. T. L.; Ding, J.; Casado, J.; Kim, D.; Wu, J. *J. Am. Chem. Soc.* **2013**, *135*, 6363. (g) Zeng, Z.; Lee, S.; Zafra, J. L.; Ishida, M.; Zhu, X.; Sun, Z.; Ni, Y.; Webster, R. D.; Li, R.-W.; López Navarrete, J. L.; Chi, C.; Ding, J.; Casado, J.; Kim, D.; Wu, J. *Angew. Chem., Int. Ed.* **2013**, *52*, 8561.
(17) Zhu, L.; Jiao, C.; Xia, D.; Wu, J. *Tetrahedron. Lett.* **2011**, *52*, 6411.
(18) (a) Lee, C. Y.; Hupp, J. T. *Langmuir* **2010**, *26*, 3760. (b) Lee, C. Y.; She, C. X.; Jeong, N. C.; Hupp, J. T. *Chem. Commun.* **2010**, *46*, 6090. (c) Chang, Y. C.; Wang, C. L.; Pan, T. Y.; Hong, S. H.; Lan, C. M.; Kuo, H. H.; Lo, C. F.; Hsu, H. Y.; Lin, C. Y.; Diau, E. W.-G. *Chem. Commun.* **2011**, *47*, 8910. (d) Wang, C.-L.; Lan, C.-M.; Hong, S.-H.; Wang, Y.-F.; Pan, T.-Y.; Chang, C.-W.; Kuo, H.-H.; Kuo, M.-Y.; Diau, E. W.-G.; Lin, C.-Y. *Energy Environ. Sci.* **2012**, *5*, 6933. (e) Ripolles-Sanchis, T.; Guo, B. C.; Wu, H. P.; Pan, T. Y.; Lee, H. W.; Raga, S. R.; Fabregat-Santiago, F.; Bisquert, J.; Yeh, C. Y.; Diau, E. W.-G. *Chem. Commun.* **2012**, *48*, 4368.
(19) Yu, L.; Muthukumaran, K.; Sazanovich, I. V.; Kirmaier, C.; Hindin, E.; Diers, J. R.; Boyle, P. D.; Bocian, D. F.; Holten, D.; Lindsey, J. S. *Inorg. Chem.* **2003**, *42*, 6629.
(20) Lewtak, J. P.; Gryko, D. T. *Chem. Commun.* **2012**, *48*, 10069.
(21) (a) Wu, J.; Gherghel, L.; Watson, M. D.; Li, J.; Wang, Z.; Simpson, C. D.; Kolb, U.; Müllen, K. *Macromolecules* **2003**, *36*, 7082. (b) Wu, J.; Pisula, W.; Müllen, K. *Chem. Rev.* **2007**, *107*, 718. (c) Grzybowski, M.; Skonieczny, K.; Butenschön, H.; Gryko, D. T. *Angew. Chem., Int. Ed.* **2013**, *52*, 9900.
(22) Page, J. A.; Wilkinson, G. *J. Am. Chem. Soc.* **1952**, *74*, 6149.
(23) Angelis, F. D.; Fantacci, S.; Selloni, A. *Nanotechnology* **2008**, *19*, 424002.
(24) Wang, P.; Zakeeruddin, S. M.; Comte, P.; Charvet, R.; Humphry-Baker, R.; Grätzel, M. *J. Phys. Chem. B* **2003**, *107*, 14336.
(25) (a) Fabregat-Santiago, F.; Garcia-Belmonte, G.; Mora-Seró, I.; Bisquert. *J. Phys. Chem. Chem. Phys.* **2011**, *13*, 9083. (b) Clifford, J. N.; Martínez-Ferrero, E.; Polomares, E. *J. Mater. Chem.* **2012**, *22*, 12415. (c) Stergiopoulos, T.; Falaras, P. *Adv. Energy Mater.* **2012**, *2*, 616.